Special Issue on Basis of Applied Sciences and Its Development in the Contemporary World
Published in Association with
Department of Technology and Organization of Construction, Samarkand State Architectural and Civil Engineering Institute, Uzbekistan
Department of Mechanization of livestock, Samarkand Institute of Veterinary Medicine, Uzbekistan
Novateur Publication India's International Journal of Innovations in Engineering Research and Technology [IJIERT]
ISSN: 2394-3696, Website: www.ijiert.org, 15th June, 2020

WIND PRESSURES COMPARISON BETWEEN WIND TUNNEL AND CFD ON SQUARE AND TRIANGLE SHAPES TALL BUILDINGS

W. S. KARRAR,
Engineer, Department of Civil, College of Engineering, Mustansiriyah, Iraq,
seerbeenkarar@gmail.com

A. M. SHAYMAA,
Associate Professor Doctor, Department of Water Resource, College of Engineering, Mustansiriyah University, Iraq, shyabed1976@gmail.com

M. JASSIM
Lecture Doctor, Department of Civil, College of Engineering, Mustansiriyah University, Iraq, Jassim_Muhsin@yahoo.com

Abstract

In the present paper the experimental and numerical study carried out on the two models of high-rise buildings under different value of wind velocity with 0 degree of wind attack. Two shapes of building namely square and triangle are considered. Pressure measurements are made on the rigid models of high-rise buildings made of timber. The models are tested in a wind tunnel. (3D) ANSYS (Fluid Fluent) was employed with finite volume method to predict the wind pressures on high-rise building using specified boundary conditions. RNG k-ε turbulence model was applied for square shape and Spalart-Allmaras turbulent model for triangle shape in order to simulate the wind turbulence. It is concluded that wind pressure resulting from wind tunnel test have a very good agreement with the wind pressure results from CFD for different value of velocity for two models. It can be seen from a comparison that the design pressure of the square model is less than the design pressure of the triangle model with different speed and the percentage of difference is about (20-25%).

Keywords: high-rise buildings, finite volume method, computational fluid dynamic (CFD), RNG κ-ε turbulence model, Spalart-Allmaras turbulence model.

Introduction

From the early times of civilization, buildings as well as tall towers smitten the humankind, the structure for such constructions were used to protect and then for ecclesiastical uses. The rapid elevation in the growth regarding modern constructions of tall buildings that started in the 1880s, was mainly for residential as well as for commercial uses. High-rise commercial buildings have been majorly considered as response to demands through businesses for being close with each other, along city centers, as achievable, thus providing extreme pressure on existing land spaces. Furthermore, due to the fact that they are forming unique landmarks, the tall commercial buildings have been often created in the city center in the sort of standing symbols with regard to the corporate organizations [8]. Certain improvements in novel techniques of construction in twentieth century established structures which are considered to be fairly lightweight, low damping, as well as flexible, that might be exposing the structures to the impact of wind actions. [8] Wind engineering can be considered as a field with the goal of majorly creating tools for better understanding regarding the fluid's action on structures with the origins, which might be marking out to 1960s. Improving the understanding with regard to this presented work encouraged the structural engineers for designing as well as ensuring the structure's performance with is the subject to wind's action to be in proper limits throughout the structure's lifetime in the structural safety as well as the serviceability criteria [7]. There have been many approaches to analyze tall buildings with regard to the wind load after utilizing building codes, wind tunnel or numerical analysis using the software. [6] examined the impact of wind flow around 3D buildings with CFD. Steady Navier-Stokes equation was solved with k-ε turbulence model in the simulation. Power-law velocity profile has been utilized to describe the incident wind. There are four value of flows were specified in this work and simulation results have been put to comparison with full-scale wind tunnel data. On the basis of such comparison, it has been specified that there has been accordance with regard to outputs which are confirming the wind flow's validation via CFD. [2] provided numerical simulation regarding the wind flow

around building of block shape with the use of 3-D turbulent flow condition. The dimensions of the model have been (30mx30mx180m. The results were compared with past CFD and with the acquired data in the boundary layer wind tunnel tests. The suggestions have been (1) inclusion regarding the turbulence in wind flow around the buildings with the use of standard k-ε turbulence model in computational process will enhance predicted velocity fields. (2) Semi-empirical k-ε turbulence model in addition to its "universal constants" underestimating the size related to recirculation zones that are utilized in eddies. (3) There are two simple modifications conducted to k-ε turbulence model decreasing the difference between computed and measured pressures on building envelope. [9] suggested wind pressure on the flat roof regarding high-rise building. Reynolds average Navier stoke equation with standard k-ε turbulence model was utilized in the modeling. The wind blowing has been suggested to be in oblique and normal directions. The estimation regarding wind pressure for 3 distinctive distance from roof edges to first grid line's center. The results specified that the roof surface might be classified in to 2 subregions on the basis of computed pressure. Furthermore, it has been indicated that oblique direction that is related to the wind blowing impacted more than normal direction in the pressure calculations. [10] investigated the modeling regarding the wind load on the tall buildings with the use of CFD. Turbulence has been provided at inlet via simulation with the use of LES with RNG-based sub grid-scale viscosity model. The dimensions of the model were (76.2x76.2x635 mm) and the computational domain dimensions were (32.5D x 15D x 3H). When compared those obtained from wind tunnel tests with CFD wind force and the moment spectra showed that an agreement between the CFD and physical simulations, and accomplished that CFD wind tests on tall buildings were a possible stand by to the conventional tests in wind tunnels. [3] examined the analysis regarding high-rise buildings which has been determined for various models of turbulent with the use of CFD and put to comparison with experimental results acquired from Tokyo Polytechnic University. A 2-D rectangular building model which has the dimensions (0.1mx0.2m) in the plan were specified for numerical simulations. The direction of wind has been specified in various angles with building walls as 0^o, 45^o& 90^o. The wind pressure

coefficients acquired from such analysis with the use of different turbulent models have been compared with wind pressure coefficients acquired from wind tunnel experiments. They have indicated that the ST k-ω turbulence model as well as the realizable k-ε turbulence model have been more efficient from the acquired results, and could examined wind forces on high raised rectangular buildings with the use of CFD simulations for various angles in the SST k-ω turbulence model as well as the realizable k-ε turbulence model. [4] compared the experimental results that is related to the numerical wind tunnel simulations regarding the wind pressures on high-rise building with from TJ-2 (Tongji University Wind-tunnel Laboratory) as well as NPL (National Physical Laboratory). Computational domain applies cylindrical computational domain, with the model of building in the center. Furthermore, radius that is related to the cylindrical computational domain (Hr) has been (10H), top of computational domain over building's roof (Ht) has been set (5H). The cylindrical computational domain has been indicated to be simple to use and there are no additional numerical errors have been provided in the case when utilized in the process of simulation. The dimensions of the first model (TJ-2) have been (102mmx152mmx610mm), also the scale ratio (1/300). The dimensions of the second model (NPL) have been (127mmx191mmx762mm) and the scale ratio (1/240). By CFD verification, as well as comparison with NPL wind tunnel experimental data and TJ-2, it has been indicated that such approach might not get great error as well as meeting the engineering requirements in modeling regarding the equilibrium atmospheric boundary layer.

The Governing Equations of Fluid

The governing equations in fluid dynamics can be applied to wind flow. Liquid or wind flows in CFD codes are governed by partial differential equations, which are based on the conservation laws for mass, energy and momentum. The following expressions are applied for three dimensional, steady and incompressible flows with constant viscosity.

$$\frac{\partial \rho}{\partial t} + \left[\frac{\partial(\rho u)}{\partial x} + \frac{\partial(\rho v)}{\partial y} + \frac{\partial(\rho w)}{\partial z}\right] = 0 \qquad \text{Continuity equation} \qquad (1)$$

$$\rho\frac{Du}{Dt} = -\frac{\partial p}{\partial x} + \frac{\partial \tau_{xx}}{\partial x} + \frac{\partial \tau_{yx}}{\partial y} + \frac{\partial \tau_{zx}}{\partial z} + \rho f_x$$ Momentum equation (2-x)

$$\rho\frac{Dv}{Dt} = -\frac{\partial p}{\partial y} + \frac{\partial \tau_{yy}}{\partial y} + \frac{\partial \tau_{yx}}{\partial x} + \frac{\partial \tau_{zy}}{\partial z} + \rho f_y$$ Momentum equation (2-y)

$$\rho\frac{Dw}{Dt} = -\frac{\partial p}{\partial z} + \frac{\partial \tau_{zz}}{\partial z} + \frac{\partial \tau_{yz}}{\partial y} + \frac{\partial \tau_{zx}}{\partial x} + \rho f_z$$ Momentum equation (2-z)

$$\tau_{xy} = \tau_{yx} = \mu\left(\frac{\partial v}{\partial x} + \frac{\partial u}{\partial y}\right)$$

$$\tau_{xz} = \tau_{zx} = \mu\left(\frac{\partial w}{\partial x} + \frac{\partial u}{\partial z}\right)$$

$$\tau_{zy} = \tau_{yz} = \mu\left(\frac{\partial v}{\partial y} + \frac{\partial w}{\partial y}\right)$$

$$\tau_{xx} = -\frac{2}{3}\mu(\nabla.V) + 2\mu\frac{\partial u}{\partial x}$$

$$\tau_{yy} = -\frac{2}{3}\mu(\nabla.V) + 2\mu\frac{\partial v}{\partial y}$$

$$\tau_{zz} = -\frac{2}{3}\mu(\nabla.V) + 2\mu\frac{\partial w}{\partial z}$$

$$\rho\frac{D}{Dt}\left(e + \frac{V^2}{2}\right) = \rho q + \frac{\partial}{\partial x}\left(k\frac{\partial T}{\partial x}\right) + \frac{\partial}{\partial y}\left(k\frac{\partial T}{\partial y}\right) + \frac{\partial}{\partial z}\left(k\frac{\partial T}{\partial z}\right) - \frac{\partial(up)}{\partial x}$$

$$-\frac{\partial(vp)}{\partial y} - \frac{\partial wp}{\partial z} + \frac{\partial(u\tau_{xx})}{\partial x} + \frac{\partial(u\tau_{yx})}{\partial y} + \frac{\partial(u\tau_{zx})}{\partial z} + \frac{\partial(v\tau_{xy})}{\partial x} + \frac{\partial(v\tau_{yy})}{\partial y} + \frac{\partial(v\tau_{zy})}{\partial z} + \frac{\partial(w\tau_{xz})}{\partial x} + \frac{\partial(w\tau_{yz})}{\partial y} + \frac{\partial(w\tau_{zz})}{\partial z} + \rho f.V$$

Energy equation (3)

Where; **ρ** is density of fluid in Kg/m^3, **u**, **v** and **w** velocities of fluid in x, y and z directions respectively in m/s, τ is the shear stress in Pa, **t** is the time in s, $\mathbf{f_x}$, $\mathbf{f_y}$ and $\mathbf{f_z}$ are the body forces in N, $\boldsymbol{\mu}$ is the molecular viscosity coefficient in Pa.s, **V** is velocity vector in m/s, **k** is the thermal conductivity, **e** is the internal energy in J , T is the temperature in C^o and **q** is the heat transferred W/m²·K.

RNG k- ε Model

Based on a mathematical technique of renormalization group, which is proposed by [11], this model is utilized to renormalize the Navier-Stokes equations and to put the effects of smaller scales of motion into account. In contrast to the standard k-ε turbulence model, the eddy viscosity is determined from a single turbulence length scale.

a) Transport equation for kinetic energy **k**:

$$\rho \frac{\partial k}{\partial t} = \frac{\partial}{\partial x_i}\left[\alpha_k \mu_{eff} \frac{\partial k}{\partial x_i}\right] - P_k + \rho\varepsilon \quad (4)$$

b) Transport equation for dissipation rate **ε**:

$$\rho \frac{\partial \varepsilon}{\partial t} - \frac{\partial}{\partial x_i}\left[\alpha_\varepsilon \mu_{eff} \frac{\partial \varepsilon}{\partial x_i}\right] - C_{1\varepsilon}\frac{\varepsilon}{k}P_k + C_{2\varepsilon}^{*}\frac{\varepsilon}{k}\rho\varepsilon \quad (5)$$

Where,

$$\mu_{eff} = \mu + \mu_t \quad (6)$$

$$\mu_t = \rho C_\mu \frac{k^2}{\varepsilon} \quad (7)$$

Where; $C_\mu = 0.0845, \alpha_k = \alpha_\varepsilon = 1.39, C_{1\varepsilon} = 1.42, C_{2\varepsilon} = 1.68$

The significant difference **(6)** between both Standard and RNG k-ε turbulence models is calculated from the near wall turbulence data as follow:

$$C_{2\varepsilon}^{*} = C_{2\varepsilon} - \frac{C_k \rho \eta^3 \left(1-\frac{\eta}{\eta_o}\right)}{1+\beta\eta^3} \quad (8)$$

Where;

$$\eta = \frac{k}{\varepsilon}\sqrt{2\, S_{ij}.S_{ij}} \quad (9)$$

$$S_{ij} = \frac{1}{2}\left(\frac{\partial u_i}{\partial x_j} + \frac{\partial u_j}{\partial x_i}\right) \quad (10)$$

$\eta_o = 4.377$

$\beta =$ *Wall damping, needs to be applied to ensure the viscosity* $= 0.01$.

ρ = the density of air, $\mathbf{u_i}$, $\mathbf{u_j}$ the velocity components, **P** is the pressure of air in Pa, **μ** is the dynamic viscosity, **t** is the time, **i**, **j** are 1, 2, 3.

The Model of the Spalart-Allmaras

This model has been advanced primarily for the aerodynamic flows in addition it is 1-equation model of turbulence. Spalart-Allmaras is an eddy viscosity transport equation. For the sake of developing a central equation closed system for flow's mean motion, one would be capable of determining the Reynolds stress distribution [5].

In general, any of the transportable scalar quantities, like the eddy viscosity, is subjected to laws of conversion, is transported based on the basic equation below:

$$\frac{DF}{Dt} = \frac{\partial F}{\partial t} + (u.\nabla)F = Deffusion + Production - Destruction \quad (11)$$

For the sake of constructing a complete turbulent flow model, each of the terms of production, diffusion and destruction have to be precisely characterized. The definition of those terms and turning them into non-dimensional will yield in some more non-dimensional and constants functions in every one of the terms.

The working variable $\breve{v}$ transport equation can be represented as:

$$\frac{\partial \breve{v}}{\partial t} + u_j \frac{\partial \breve{v}}{\partial x_j} = C_{b1}\breve{S}\breve{v} + \frac{1}{\sigma}\left[\frac{\partial}{\partial x_j}(v + \breve{v})\frac{\partial \breve{v}}{\partial x_j} + C_{b2}\frac{\partial^2 \breve{v}}{\partial x_j^2}\right] - C_{w1}f_w(\frac{\breve{v}}{d})^2 \quad (12)$$

The eddy viscosity can be represented as:

$$\mu_t = \rho\breve{v}f_{v1} \quad (13)$$

In log layer, we can say that is $\breve{v} = kyu_\tau$, which is why in the layer of the buffer and viscous sub layer as well. The function of damping f_{v1} can be represented as:

$$f_{v1} = \frac{\chi^3}{\chi^3 + C_{v1}^3} \quad (14)$$

Where; $\chi^3 = \frac{\breve{v}}{v}$

$$\breve{S} = \sqrt{2\,\Omega_{ij}\Omega_{ij}}f_{v3} + \frac{\breve{v}}{k^2 d^2}f_{v2} \quad (15)$$

Where, $\Omega_{ij} = \frac{1}{2}(\frac{\partial u_i}{\partial x_i} - \frac{\partial u_j}{\partial x_j})$; $f_{v2} = 1 - \frac{\chi}{1-\chi f_{v1}}$; $f_{v3} = 1$.

For the sake of obtaining a faster behavior of the decaying of the destruction in the external boundary layer area, function f_w is utilized as:

$$f_w(g) = g(\frac{1+C_{w3}^6}{g^6 + C_{w3}^6})^{\frac{1}{6}} \quad (16)$$

Where, $g - r + C_{w2}(r^6 - r)$ and $r - \frac{\breve{v}}{k^2 d^2 \breve{S}}$

$C_{b1} = 0.1355$, $C_{b2} = 0.622$, $\sigma = \frac{2}{3}$, $C_{v1} = 7.1$, $C_{w2} = 0.3$, $C_{w3} = 2$.

$C_{w1} = \frac{C_{b1}}{k^2}\left(\frac{1+C_{b2}}{\sigma}\right)$, $k = 0.41$.

Experimental Work

Description of the Prototype Building with Square Cross-Section

The geometric scale of building model is chosen to maintain the equality of ratios of overall building dimensions to the inveterate lengths of the generated wind model. These inveterate

lengths may be roughness length of terrain and the boundary layer depth etc. In selecting model's scale, there is high importance in avoiding the impact regarding wind tunnel walls as well as extravagant blockage of the test section. The dimensions of this model are (100x100x250 mm) as shown in (**Figure 1**). Eleven pressure ports are made on center of two faces of building model for measurement of wind pressures and are shown in (**Figure 1**). The pressure ports are the same number and location in the two faces. The first face is the windward face and the second face is the leeward face. The distance between the pressure points are shown in the (**Figure 2**). Wind direction on model are as indicated in the (**Figure 3**). The experimental model is manufactured from wood plate, where the thickness of plate was 15 mm for four sides of the model. The wood plate connection seams were filled with wood putty to ensure smooth wind flow over the seams. The building has circular base made from wood plate with diameter 250 mm and 4 mm thickness. The model is open from the base for producing air pressure measuring tubes while it is closed from the top by using a 4 mm thick wood panel and with the same cross-section dimension of the model itself. The laboratory-building model that has been used in experimental is shown in (**Plate 1**).

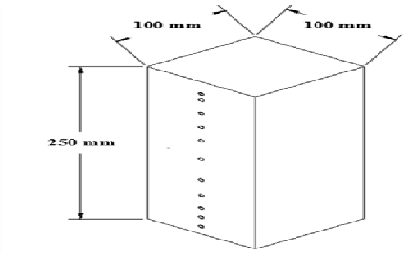

Figure (1) Dimensions and Pressure Ports of Square High-rise Building Model.

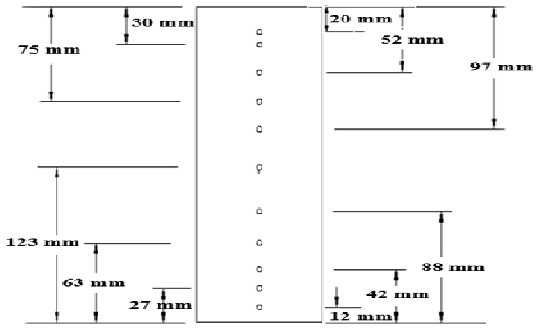

Figure (2) The Distance of the Pressure Ports on the Model.

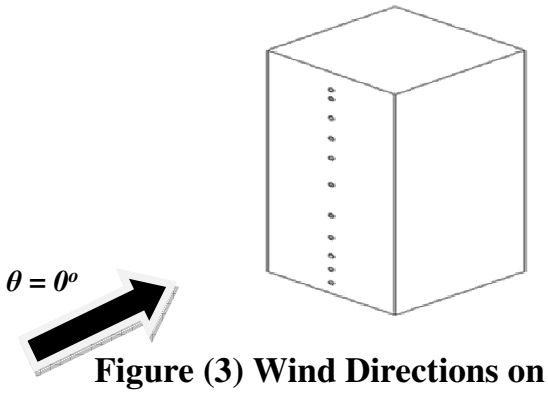

Figure (3) Wind Directions on Model.

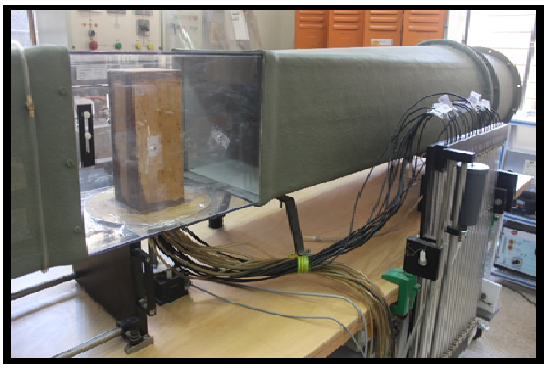

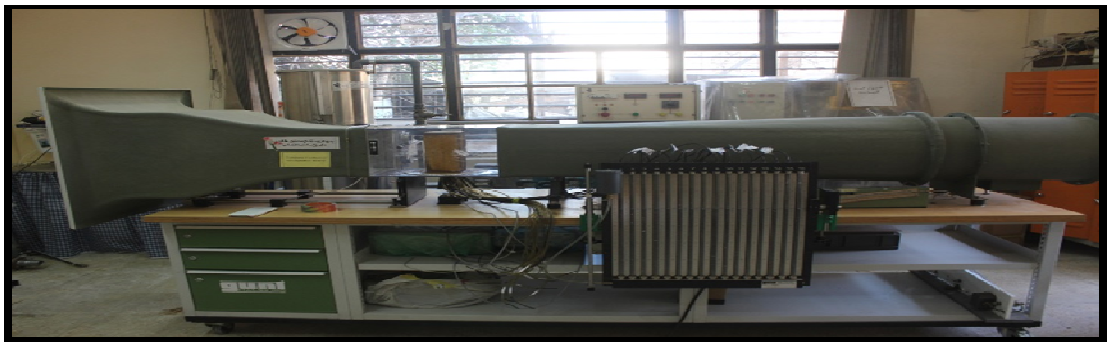

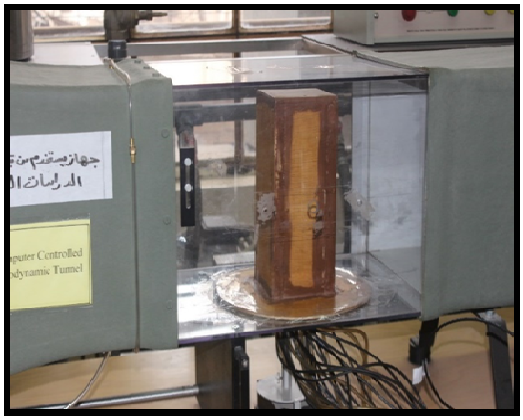

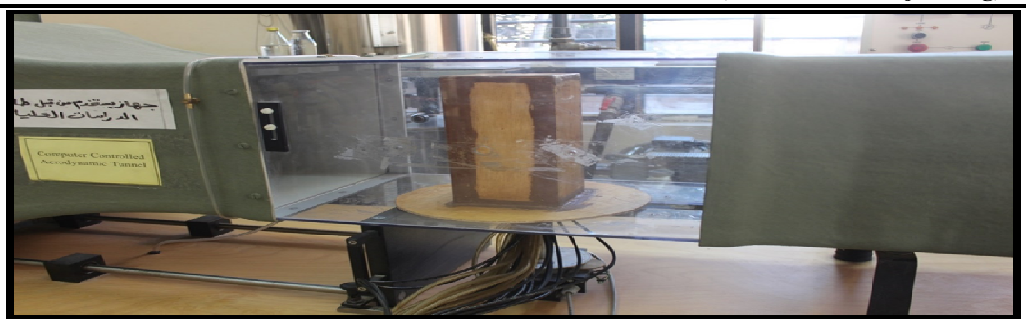

Plate (1) Photographs Showing the Laboratory Horizontal Wind Tunnel Square Cross-section Model.

Description of the Prototype Building with Triangle Cross-Section

The geometric scale of building model is chosen in the same way of the first model. The dimensions of the sides' triangle model are (100x100x150 mm) and (250 mm) height as are shown in (**Figure 4**). Five pressure ports are installed on the center of two faces of building model for measurement of wind pressures shown in (**Figure 4**). The pressure ports are the same number and location of the two faces. The distance of the pressure ports is indicated in the (**Figure 5**). Wind direction on model as shown in the (**Figure 6**). The experimental model is manufactured from wood plate, where the thickness of plate was 15 mm for two sides of the building and 4 mm for the other side. The wood plate connection seams were filled with wood putty to ensure smooth wind flow over the seams. The building has circular base made from wood plate with diameter 250 mm. It is open from the base for producing air pressure measuring tubes. The building is closed from the top using a 4 mm thick wood panel and with the same dimension of the building itself. The laboratory-building model that has been used in experimental is shown in (**Plate 2**).

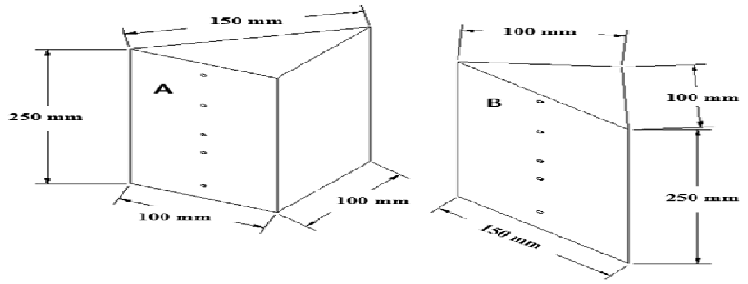

Figure (4) Dimensions and Pressure Ports of Triangle Tall Building Model.

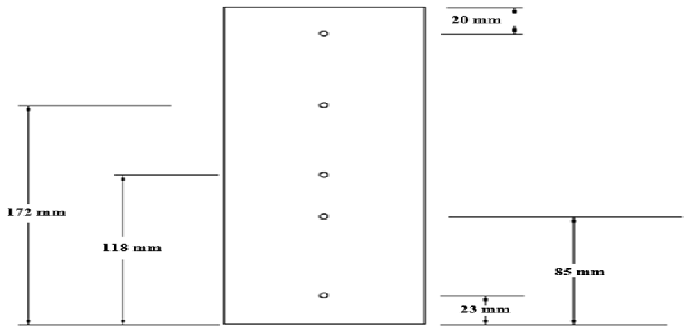

Figure (5) Distance of the Pressure Ports for Two Faces on the Model.

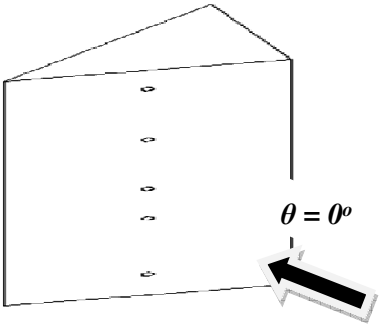

Figure (6) Wind Directions on Model.

Plate (2) Photographs Showing the Laboratory Horizontal Wind Tunnel Triangle Cross-section Model.

Laboratory Wind Tunnel

The experimental test is conducted in wind tunnel with dimension LxWxH: 2870 x 890 x 1540 mm and the weight of the wind tunnel is 250kg. The flow cross-section WxH: 292x292 mm and with length 450 mm. as shown in **(Plate 3a, 3b)** that describes the wind tunnel with the building models receptivity. The wind velocity was varying from 1 to 27 m/s. The wind tunnel components are illustrated in **(Figure 7)**.

The bed and sidewalls of wind tunnel are made from smooth strong glass. Every model is placed in wind tunnel at center of measurement section. Wind velocity used in the test is 16, 20 and 24 m/s.

Plate (3a) The Laboratory Wind Tunnel with the First Model.

Plate (3b) The Laboratory Wind Tunnel with the Second Mode. Plate (3) Photographs Showing the Laboratory Wind Tunnel with: (A) First Model, (B) Second Model.

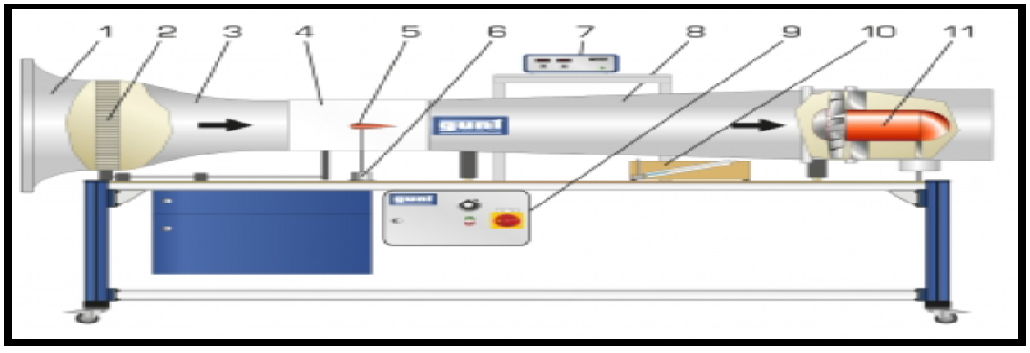

1 inlet contour, 2 flow straightener, 3 nozzle, 4 measuring section, 5 model, 6 force sensor, 7 display and control unit, 8 diffuser, 9 switch cabinet, 10 inclined tube manometer, 11 axial fan Figure (7) Components of the Wind Tunnel.

Measured of Pressure

In the laboratory wind tunnel, sixteenth manometer tubes with a diameter of 5 mm are used to record the pressure head at pressure ports on the square and triangle model. The liquid that was used in the manometer is the water. The mass density of water (ρw) is 1000 kg / m^3. The pressure ports are a small copper pipe with approximately diameter 1 mm and 25 mm length that is used for the models tests. In addition, they are connecting with the model by using glue. These pressure ports transport the wind pressure from them to manometer by tubes to measure the pressure head. The pressure head convert to pressure by using **Eq. (17)**.

$$P = \rho\,(\Delta h)\,g \qquad (17)$$

Where; P is the pressure in N/m^2, g represent acceleration caused by gravity in m/s^2, Δh represent pressure head in meters and ρ represent the water's density in kg/m^3.

CFD Simulation Model

The optimum mesh sizes that selected to be adequately modeled the wind flow over building model was having 1 mm for edges and 5 mm for face. The flow around the building model is shown (**Figure 8**) . The unstructured mesh scheme is applied in this paper as shown (**Figure 9**). The number of elements for square and triangle model are about 745x10^3 and 748x10^3 respectively.

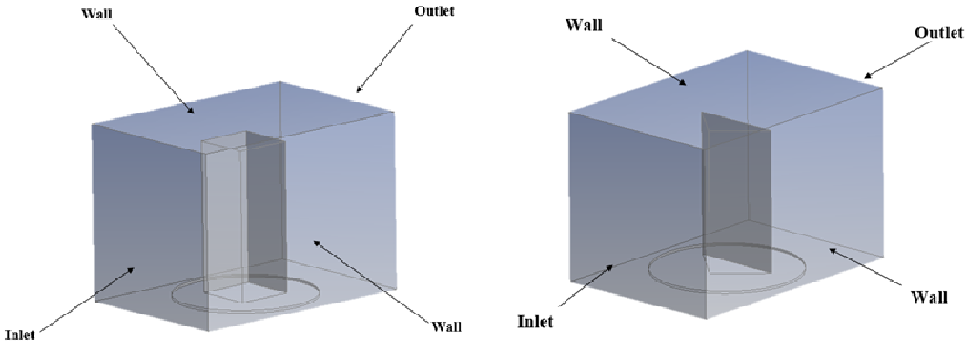

Figure (8) the Boundary Conditions of the Models Study.

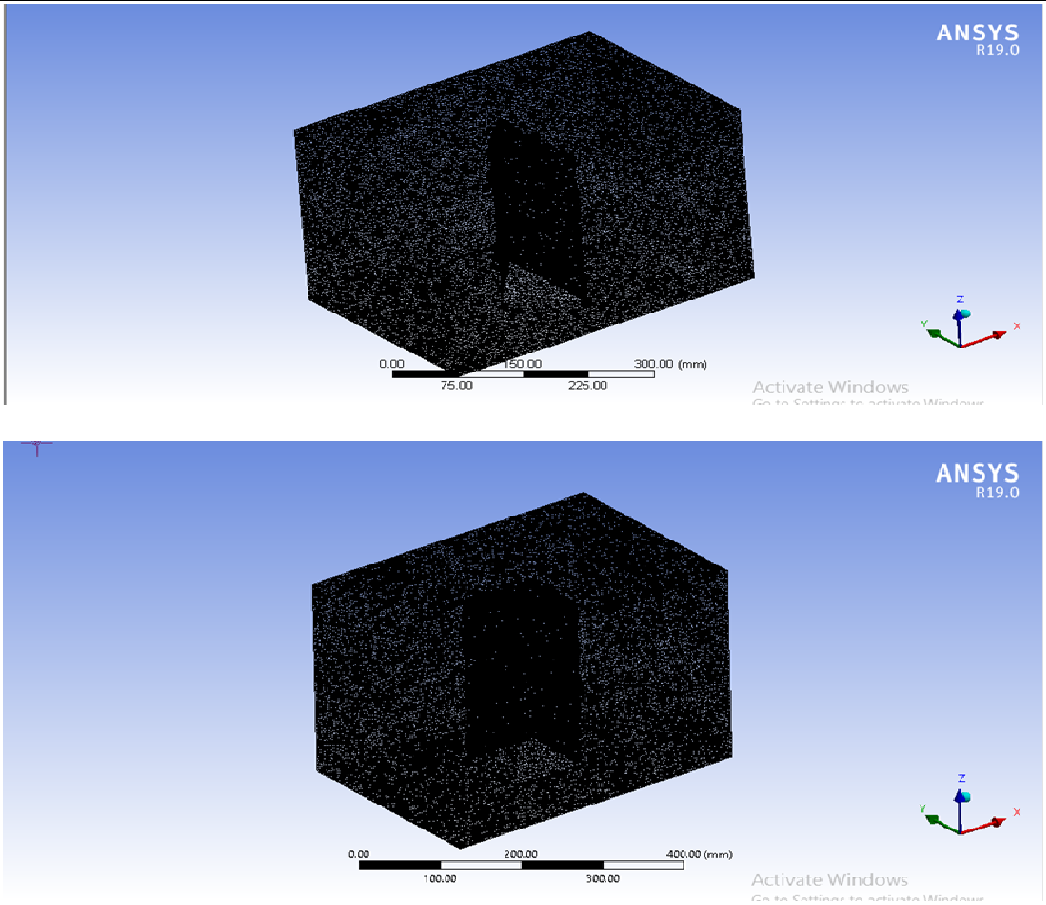

Figure (9) Mesh Generation for Two Models.

Pressure Results of Prototype Building with Square Cross-Section

Figure (10), **(12)** and **(14)** indicated the results of pressure for windward, while **Figure (11)**, **(13)** and **(15)** shown the results of pressure for leeward for different value of wind velocity (16, 20 and 24 m/s). **(Figure 16)** shown the pressure contour and velocity streamline results for model. Relative errors for the pressure between numerical and experimental results are generally for model is 0.1% to 5.22%. It can be seen from (**Figure 16**) of velocity distribution for model that the speed on the practical side is the same on the theoretical side and starts to change when exposed to friction. It can be indicated that the wind distribution on the model shows not slight change in speed as the shape of the square building increase friction and makes the change in speed very large.

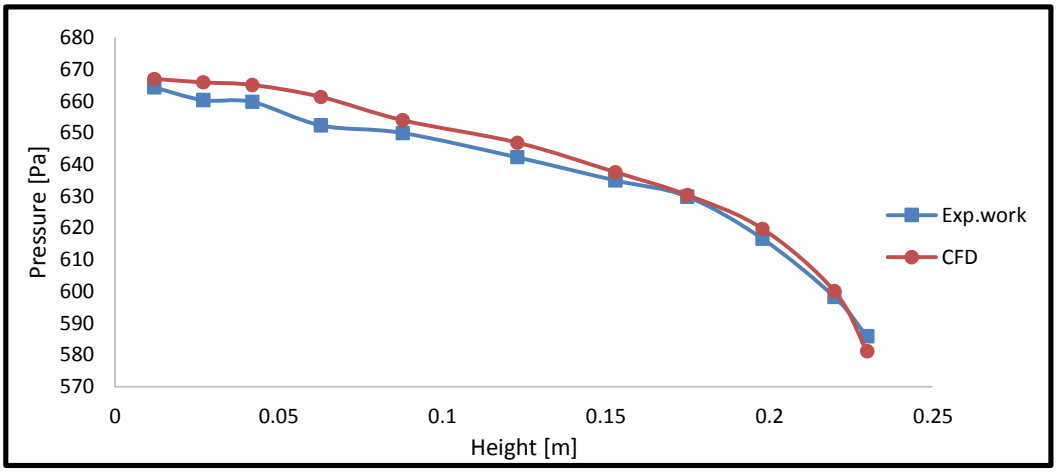

Figure (10) Comparison between Pressures Obtained by Experimental and Numerical Models for Windward for 16 m/s Wind Speed.

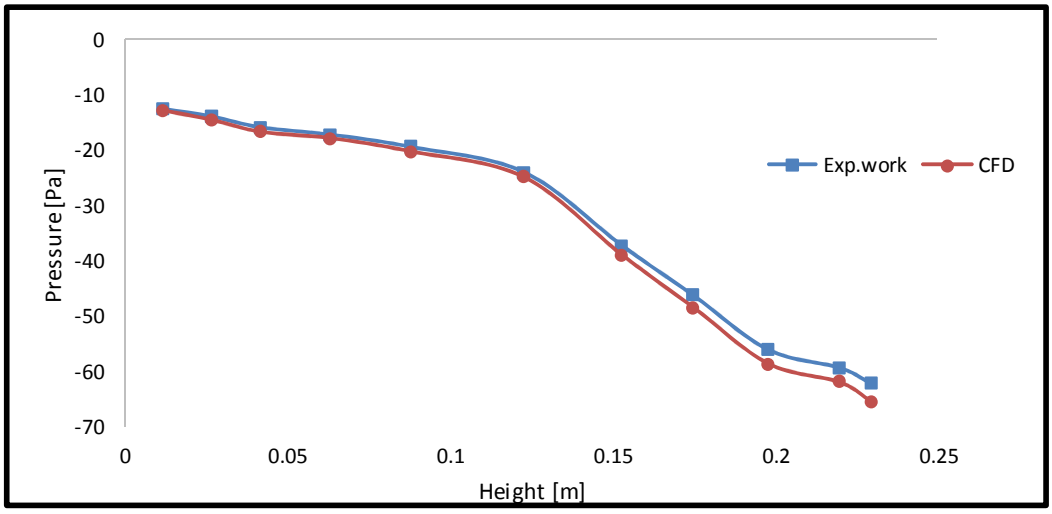

Figure (11) Comparison between Pressures Obtained by Experimental and Numerical Models for Leeward for 16 m/s Wind Speed.

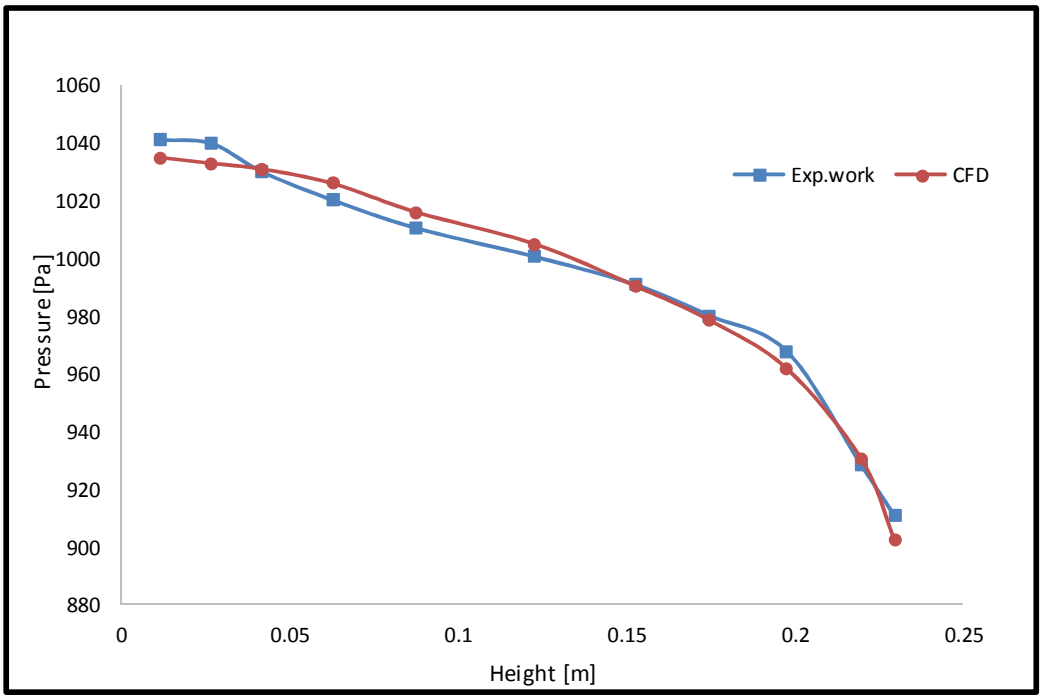

Figure (12) Comparison between Pressures Obtained by Experimental and Numerical Models for Windward for 20 m/s Wind Speed.

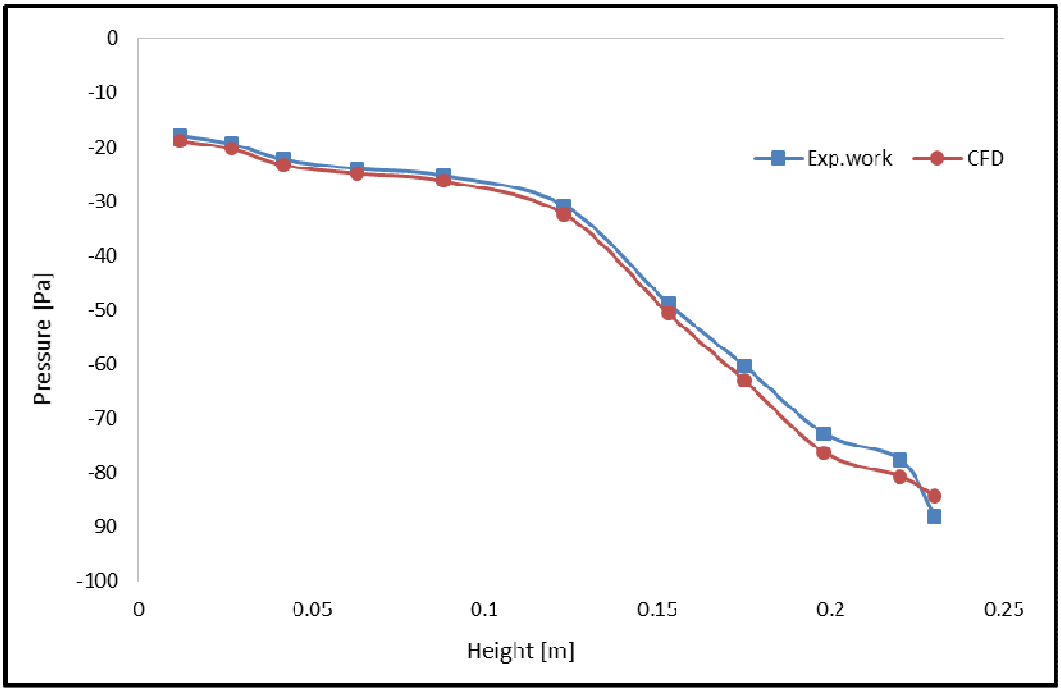

Figure (13) Comparison between Pressures Obtained by Experimental and Numerical Models for Leeward for 20 m/s Wind Speed.

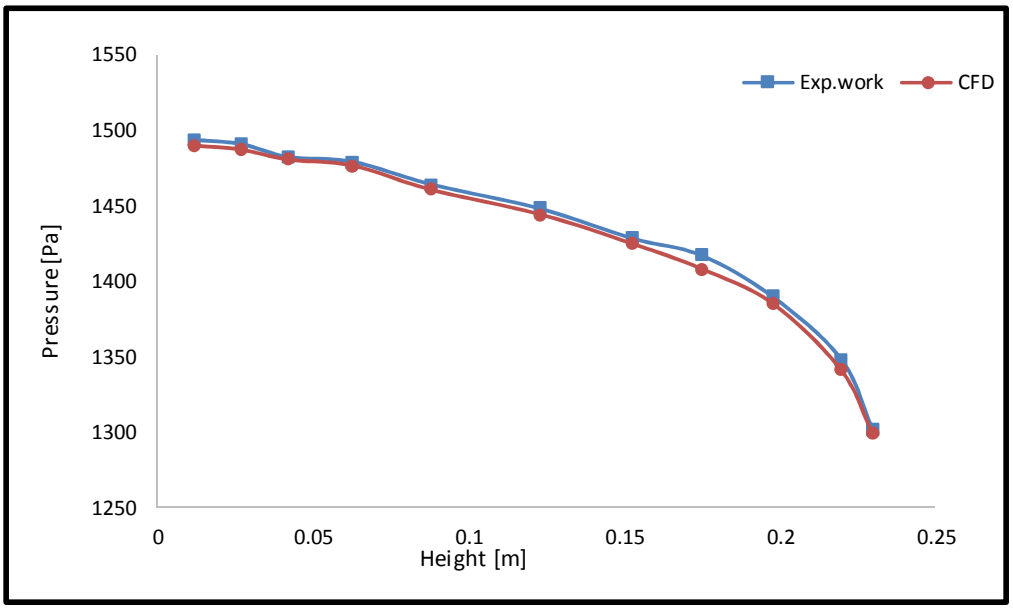

Figure (14) Comparison between Pressures Obtained by Experimental and Numerical Models for Windward for 24 m/s Wind Speed.

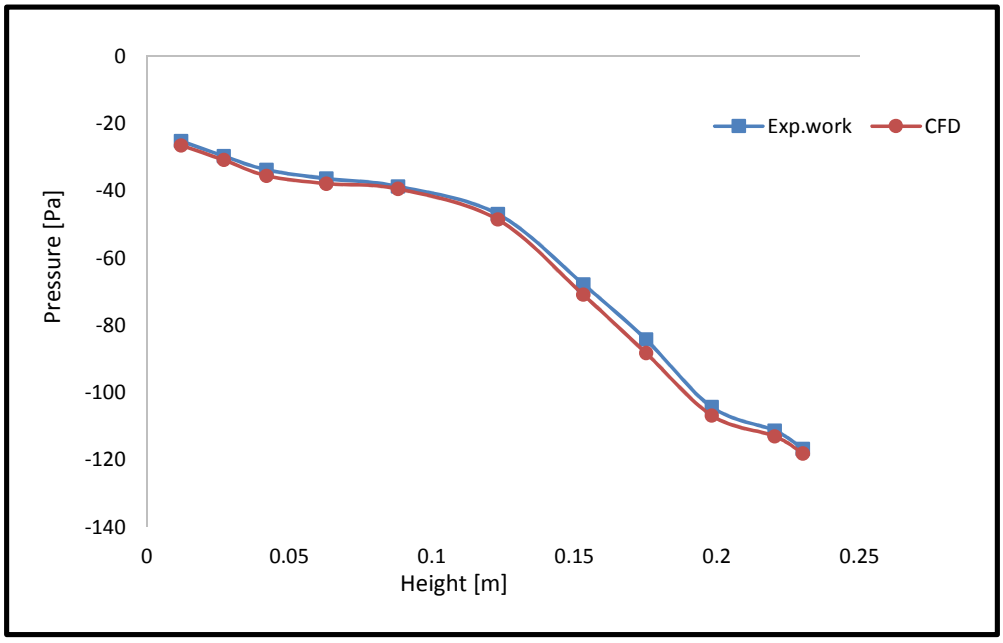

Figure (15) Comparison between Pressures Obtained by Experimental and Numerical Models for Leeward for 24 m/s Wind Speed.

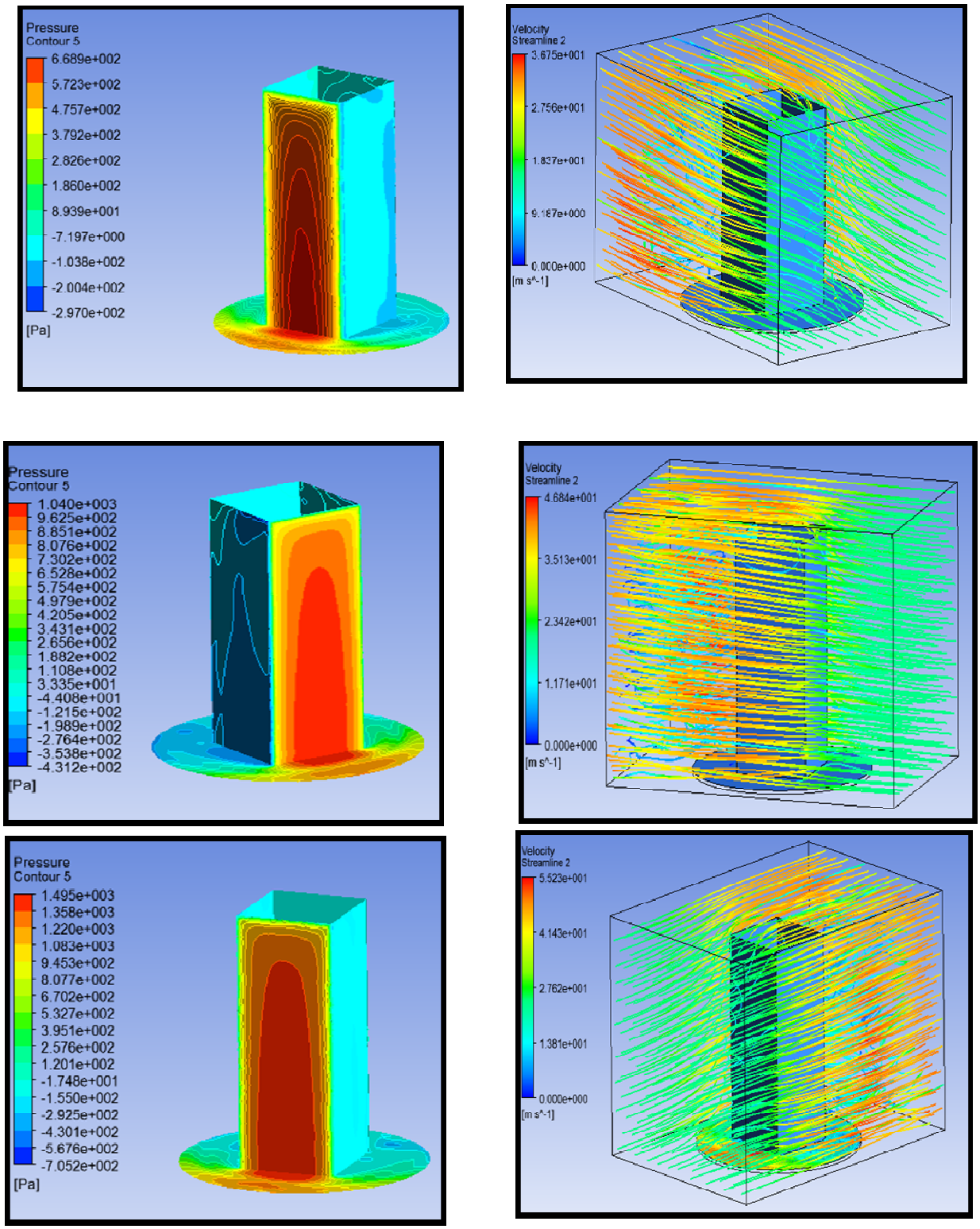

Figure (16) Pressure Contour and Streamline Velocity for Square Model with Different Velocity.

Pressure Results of Prototype Building with Triangle Cross-Section

Figure (17), **(19)** and **(21)** indicated the results of pressure for (face A), while **Figure (18)**, **(20)** and **(22)** shown the results of pressure for (face B) for different value of wind velocity (16, 20 and 24 m/s). **(Figure 23)** shown the pressure contour and velocity streamline results for model. Relative errors for the pressure between numerical and experimental results are generally for model is 0.12% to 5.20%. It can be seen from (**Figure 23**) below of velocity distribution for model that the speed on the practical side is the same on the theoretical side and starts to change when exposed to friction. It can be indicated that the wind distribution on the model shows not slight change in speed as the shape of the triangle building increase friction and makes the change in speed very large.

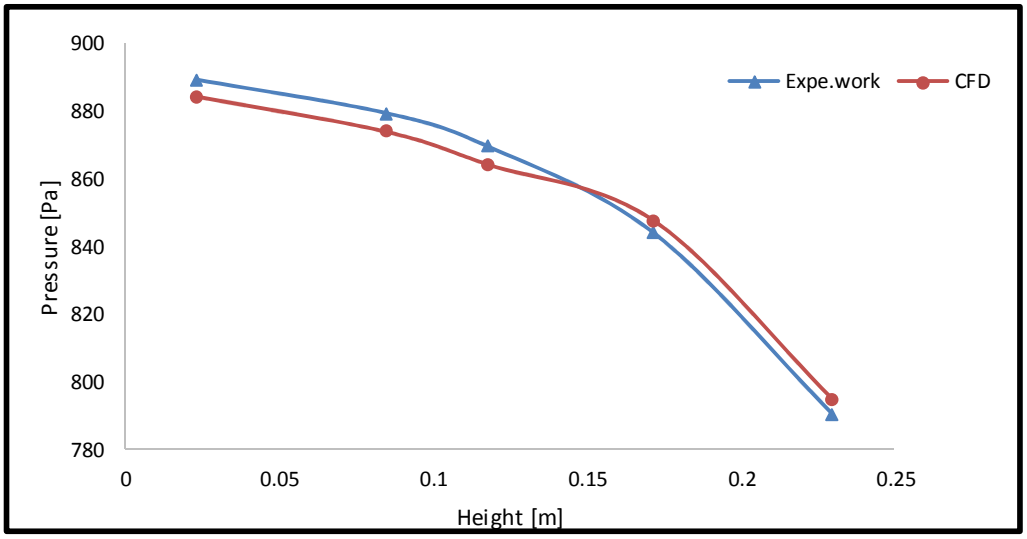

Figure (17) Comparison between Pressures Obtained by Experimental and Numerical Models for (Face A) for 16 m/s

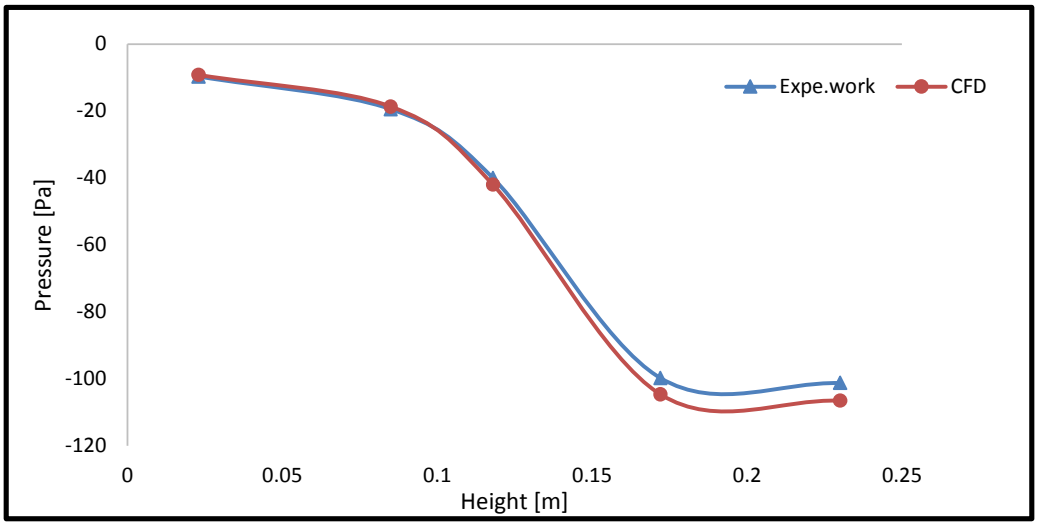

Wind Speed.

Figure (18) Comparison between Pressures Obtained by Experimental and Numerical Models for (Face B) for 16 m/s Wind Speed.

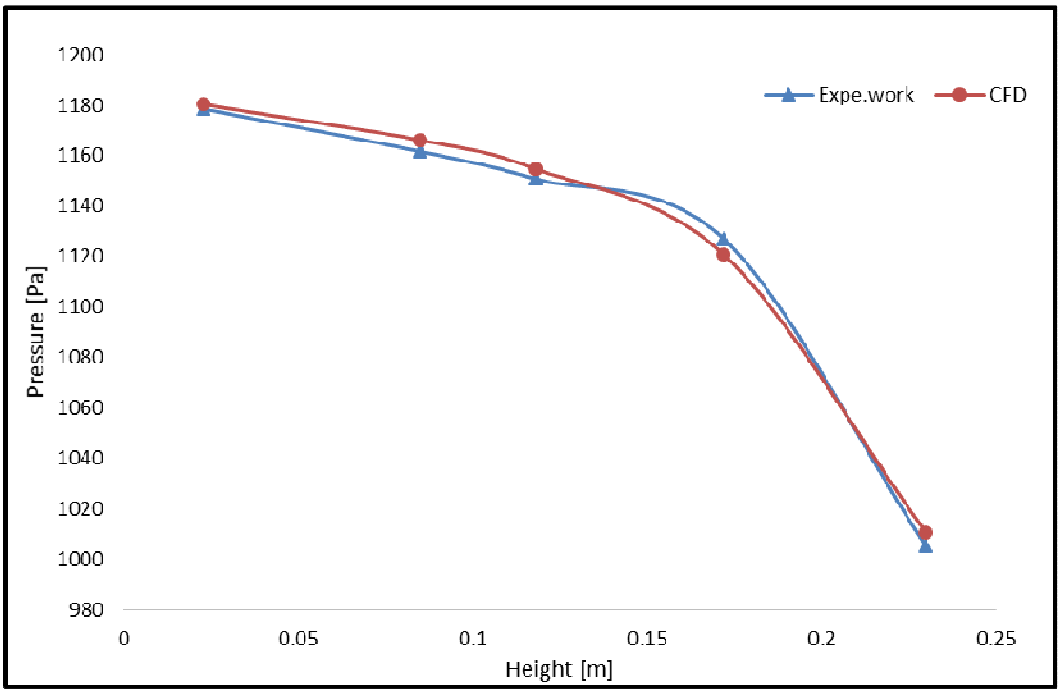

Figure (19) Comparison between Pressures Obtained by Experimental and Numerical Models for (Face A) for 20 m/s Wind Speed.

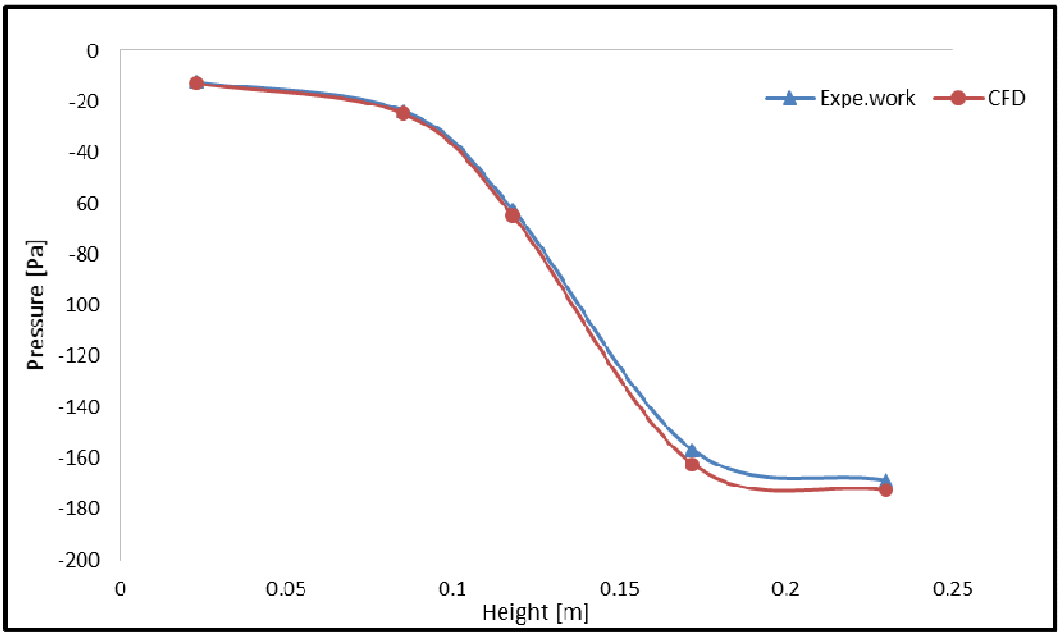

Figure (20) Comparison between Pressures Obtained by Experimental and Numerical Models for (Face B) for 20 m/s Wind Speed.

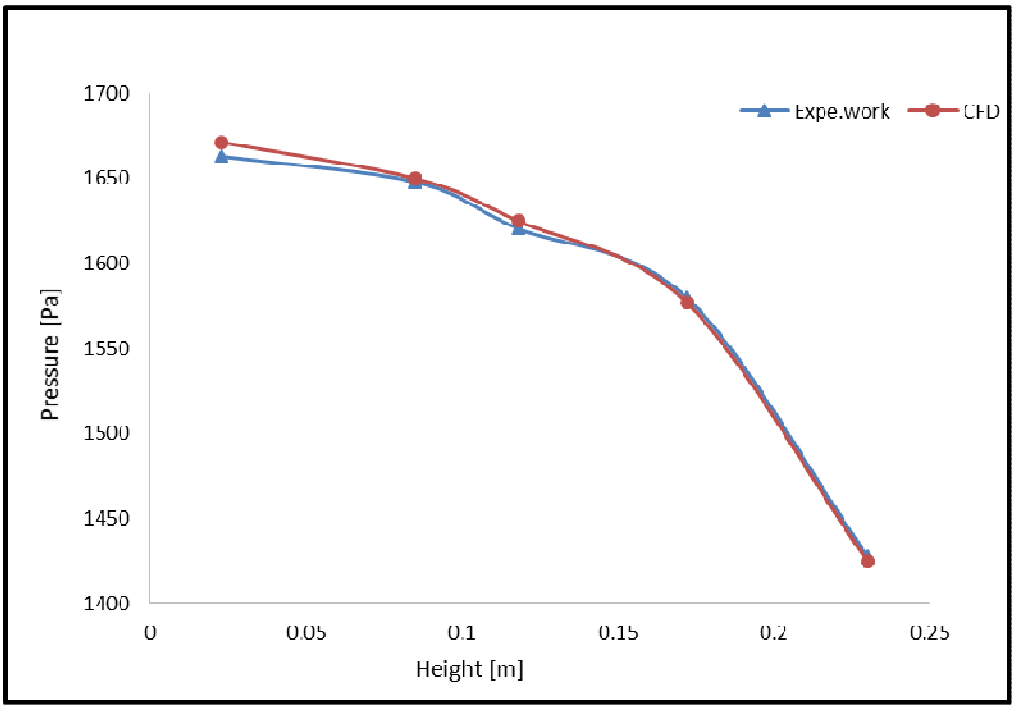

Figure (21) Comparison between Pressures Obtained by Experimental and Numerical Models for (Face A) for 24 m/s Wind Speed.

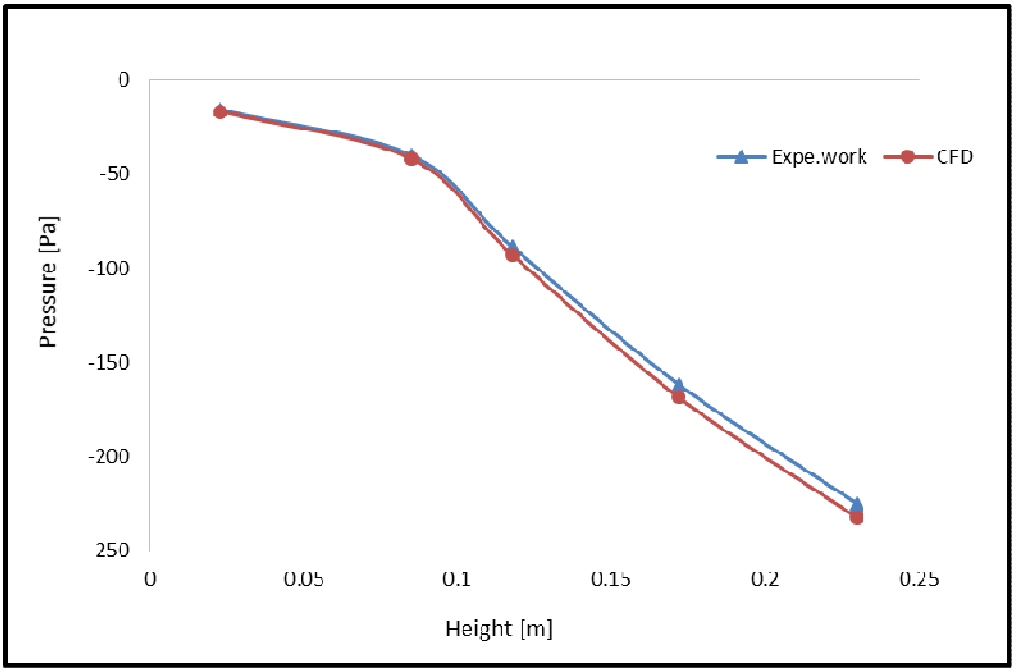

Figure (22) Comparison between Pressures Obtained by Experimental and Numerical Models for (Face B) for 24 m/s Wind Speed.

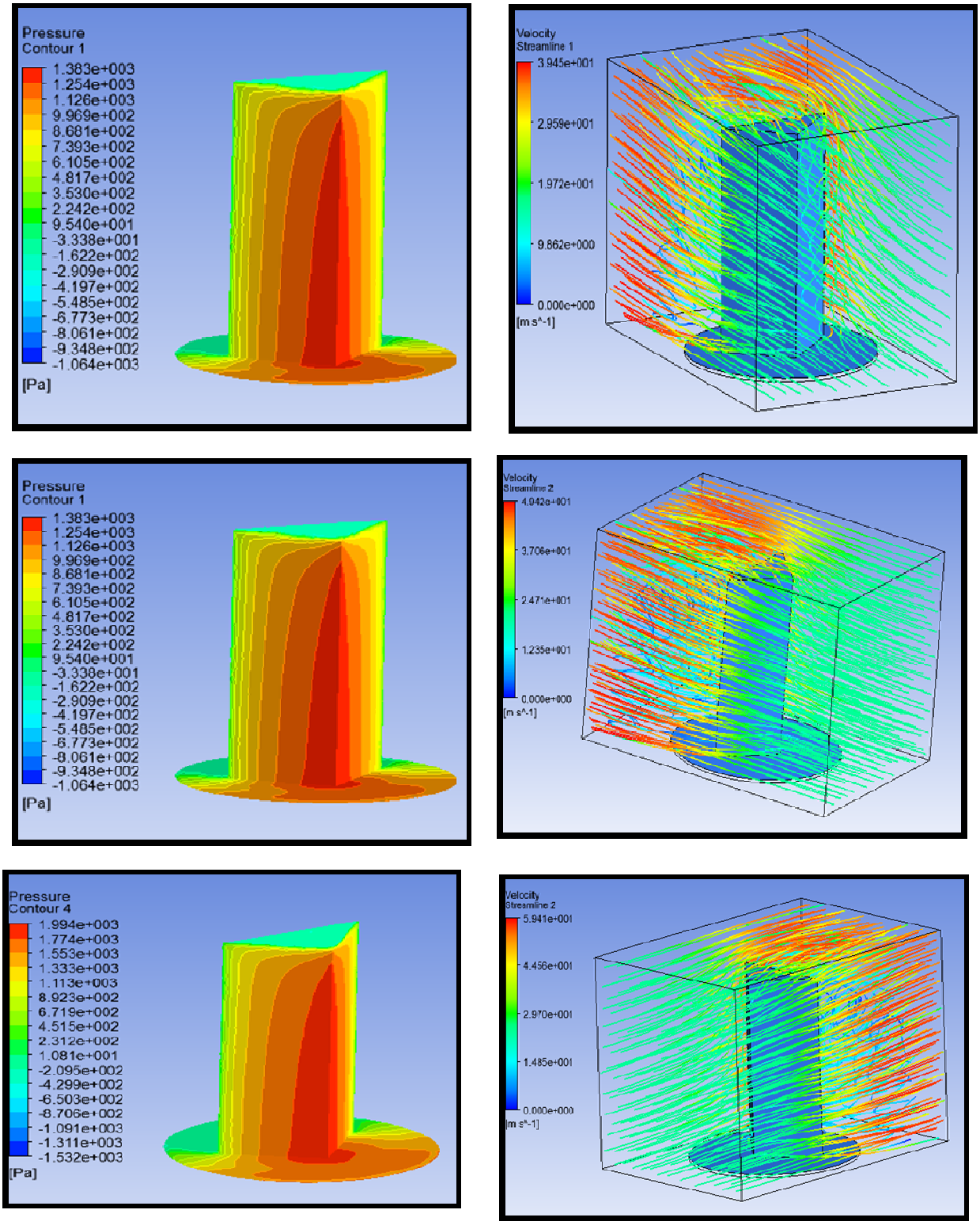

Figure (23) Pressure Contour and Streamline Velocity for Triangle Model with Different Velocity.

Design Pressure Comparison for Two Models and Effect of Its Shape on Result

Based on numerical results, the design pressure is calculated for two models. (**Figure 24**) show a comparison of the design pressure results of two models with height of model for three different velocities. It can be see that the design pressure of the square model is less than the design pressure of the triangle model with different speed and the percentage difference is about (20-25%).

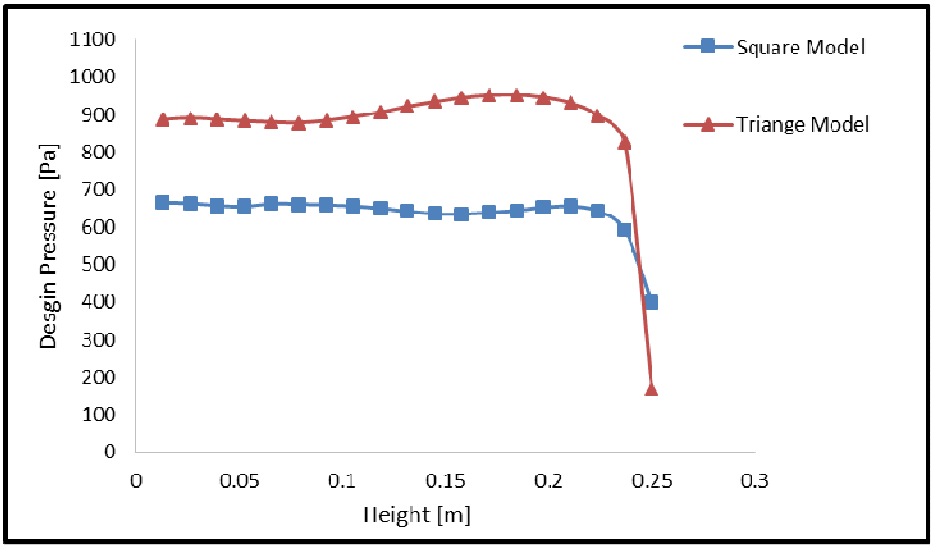

Figure (24a) for 16 m/s Velocity.

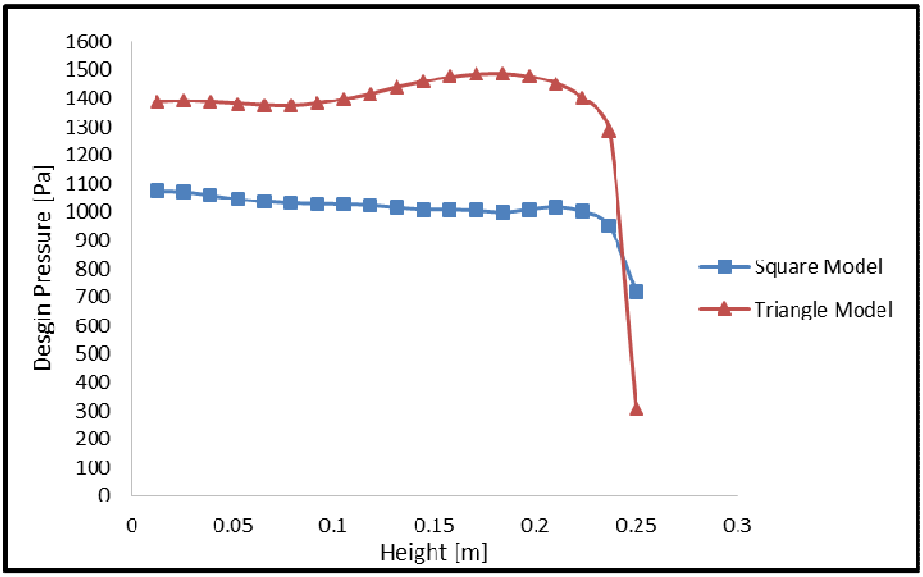

Figure (24b) for 20 m/s Velocity.

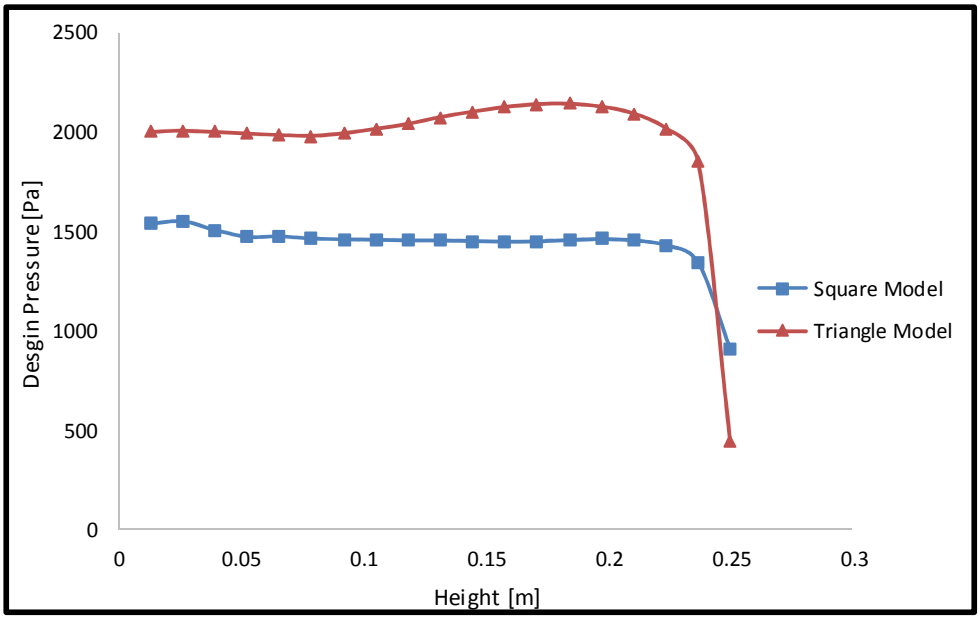

Figure (24c) for 24 m/s Velocity. Figure (24) Design Pressure Comparison between Square and Triangle Models with Different Wind Velocity.

It can be observed from the (**Figure 16**) and (**Figure 23**) of streamline velocity and pressure contour of two models the pressure changes with the height gradually, in the case of the two models decreases with the height slightly, knowing that the wind speed is fixed with the height. It might be indicated that there will be increase in pressure with the increase in wind speed and It can be shown that the pressure results of the square model less than the pressure results for the triangle model. The reason for this difference with the stability of speed and the angle of the wind is that the surface area of the square model over which the wind is located is less than the surface area of the triangle model. We note that the forward pressure has a positive signal and we note the back side of the model with a negative signal, which means that the pressure is withdrawn. It can be concluded that the square-shaped model of the building is appropriate in this case when choosing between two models.

Conclusion

In this, paper the pressure results comparison between the CFD simulation and wind tunnel test shows that:

1. Computational fluid dynamics simulation can be used to estimate the pressure on surface of models instead of wind tunnel test.

2. Using computational fluid dynamics instead of wind tunnel test is economical because it is inexpensive.

3. The wind tunnel is not able to test some complex models, but computational fluid dynamics can test any model, no matter how complex.

4. Outputs through the diaphragm are better than wind tunnel screening, as a full report of the checkup process and the input and output process can be done better than examining the costly wind tunnel.

5. By comparing the models with each other, it was found that the square section-building model is better than the triangle section-building model when the same wind speed is affected on them in the same direction due to the difference in the surface area over which the wind is given. The square model gave less design pressure to the triangle model and thus we can conclude that a study can be done to find the best shape of a building to resist the wind forces, as well as distribute pressure on the sides of the building in a simple way using CFD.

References

[1] ANSYS, Inc. (2013). ANSYS FLUENT Theory Guide. Release 18.2, 15317(November), 373–464.

[2] Baskaran, A., & Stathopoulos, T. (1989). Numerical evaluation of wind effects on buildings. Building and Environment, 24(4), 325–333.

[3] Rajkamal and Ch. Raviteja. (2016). Analysis of Wind Forces on a High-Rise Building by RANS-Based Turbulence Models using Computational Fluid Dynamics. (09), 28–34.

[4] Han, Z., Wang, X., & Zhao, D. (2017). Wind Pressure on High-rise Buildings : A Numerical Simulation of Computational Domain. Journal of Civil Engineering Research, 7(2), 46–52.

[5] Kostić, Č. (2016). Review of the Spalart-Allmaras turbulence model and its modifications to three-dimensional supersonic configurations. Scientific Technical Review, 65(1), 43–49.

[6] Paterson and Colin Apelt. (1986). "Computation of wind flows over three-dimensional buildings." Journal of Wind Engineering and Industrial Aerodynamics 24(3), 193–213.

[7] Simiu, E., Scanlan, R. H. (1978). Wind Effects on Structures, John Wiley & Sons, New York, N.Y.

[8] Smith Brayan Stafford and Coull Alex. (1991). Tall Building strctures: Analysis and Design.

[9] Stathopoulos and Zhou. (1995). "Numerical evaluation of wind pressures on flat roofs with the k-ε model." Building and Environment, Volume 30(Issue 2), Pages 267-276.

[10] Ton Thi Tu Anh. Modeling of Wind Load on Tall Buildings Using Cfd, National University of Singapore. , (2004).

[11] Yakhot, V., Orszag, S. A., Thangam, S., Gatski, T. B., & Speziale, C. G. (1992). Development of turbulence models for shear flows by a double expansion technique. Physics of Fluids A, 4(7), 1510–1520.